ASTEROSEISMIC INFERENCE FOR SOLAR-TYPE STARS

M.J.P.F.G. Monteiro[1], J. Christensen-Dalsgaard[2], and M.J. Thompson[3]

[1]Departamento de Matemática Aplicada da Faculdade de Ciências, and
Centro de Astrofísica da Universidade do Porto, Rua das Estrelas, P-4150-762 Porto, Portugal
[2]Teoretisk Astrofysik Center, Danmarks Grundforskningsfond, and
Institut for Fysik og Astronomi, Aarhus Universitet, DK-8000 Aarhus C, Denmark
[3]Department of Physics, Imperial College, London, England

Abstract

The oscillation spectra of solar-type stars may in the not-too-distant future be used to constrain certain properties of the stars. The CD diagram of large versus small frequency separations is one of the powerful tools available to infer the properties – including perhaps masses and ages – of stars which display a detectable spectrum of oscillation. Also, the border of a convective region in a solar-type star gives rise to a characteristic periodic signal in the star's low-degree p-mode frequencies. Such a signature contains information about the location and nature of the transition between convective and non-convective regions in the star.

In this work we address some of the uncertainties associated with the direct use of the CD diagram to evaluate the mass and age of the star due to the unknown contributions that make the stars different from the evolutionary models used to construct our reference grid. We also explore the possibility of combining an *amplitude versus period* diagram with the CD diagram to evaluate the properties of convective borders within solar-type stars.

Key words: asteroseismology; solar-type stars; stellar evolution; convection

1. Introduction

Seismology of solar-type stars besides the Sun is expected in the not-too-distant future to provide information of great relevance for understanding stellar evolution, and here we address the topic of using the frequencies of oscillation of a few models of solar-type stars in order to constrain their structure.

The asteroseismic HR diagram (also called the "CD diagram") is one of the powerful tools available to infer the properties of stars which display a detectable spectrum of oscillation. The CD diagram utilises the so-called large and small frequency separations (defined in Section 2), which are relatively easily identifiable characteristics of solar-type stars. Together they may provide information on a star's mass and age (e.g. Christensen-Dalsgaard 1993b). However, as noted by Gough (1987), such inferences are affected by other unknown aspects of the stellar properties; also, the errors in the observed frequencies must evidently be taken into account.

Another aspect of a solar-type star's frequency spectrum is that the border of a convective region (or indeed any other sharp variation) gives rise to a characteristic periodic signal in the low-degree p-mode frequencies.

In this work we use a grid of reference models both to construct a CD diagram and to calibrate the behaviour of the oscillatory signal from the base of the convective envelope (the amplitude versus period diagram) for stars of different masses and ages. Further, we address some of the uncertainties associated with the direct use of the CD diagram by considering grids of stellar models with different input physics. To illustrate the combined application of these tools, and to test the reliability of our inferences, in this paper we perform a blind test on frequency data from three stellar models, supplied by one author to another.

2. Properties of the frequencies

The easiest information to measure from the frequencies of oscillation of other stars is the *large frequency separation*. This quantity is the regular spacing between modes of same degree and consecutive order,

$$\Delta\nu_{n,l} \equiv \nu_{n+1,l} - \nu_{n,l} \ , \tag{1}$$

where $\nu_{n,l}$ is the frequency of the mode of order n and degree l. The large separation is mainly a measurement of the sound travel time between the surface of the star and the centre:

$$2\int_0^R \frac{\mathrm{d}r}{c} \ ; \tag{2}$$

however $\Delta\nu_{n,l}$ is a function of frequency. Other aspects also contribute to its value, besides the different sensitivity of the modes to the global structure of the star.

The *small frequency separation* is defined according to

$$\delta\nu_{n,l} = \nu_{n,l} - \nu_{n-1,l+2} \ . \tag{3}$$

The small separations are sensitive to evolutionary changes in the structure of the core. That makes this quantity sensitive to the age of the star as determined by the central hydrogen abundance X_c.

Sharp variations of the structure produce in the modes of oscillation a characteristic perturbation that is proportional to the amplitude of the mode at that location. This corresponds to a signal superimposed in the frequencies

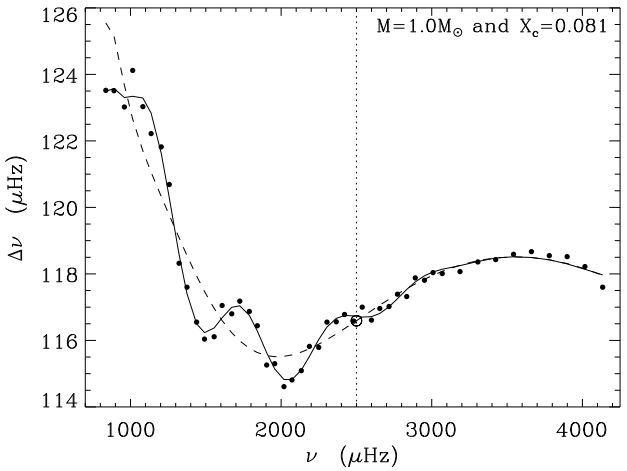

Figure 1. Large frequency separations for one model. The continuous line is a fit to the points, while the dashed line is the component of that fit that corresponds to powers of $(1/\nu)$. The difference is the contribution $\Delta\nu_b$ to the frequency differences due to the presence of the second helium ionization zone near the surface of the star. The value at ν=2500μHz has been defined as the representative value of the separation and is indicated as an open circle.

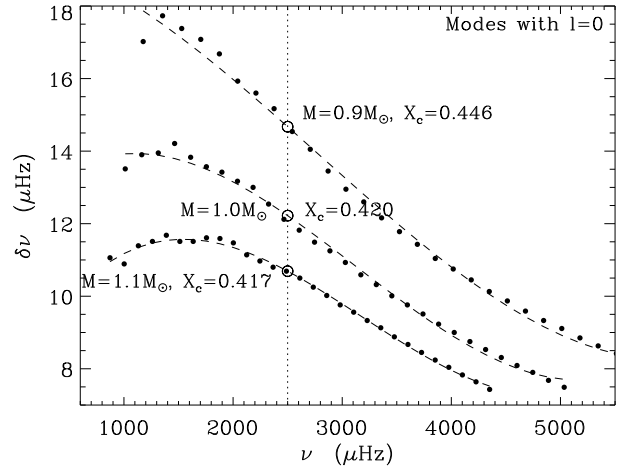

Figure 2. Small frequency separations $\delta\nu_{n,0}$ for three models. The dashed line corresponds to a fit of the points with an expansion in powers of $1/\nu$. In order to find the value of $\delta\bar{\nu}$ we use the value of the fit at ν=2500μHz.

which is periodic and with the amplitude measuring the sharpness of the transition. Of particular note for solar-type stars are the signal from the base of the convective envelope and that from the second helium ionization zone. Such a signal has been used with success for studying the base of the convection zone in the Sun (Basu et al. 1994, Monteiro et al. 1994, Roxburgh & Vorontsov 1994; Christensen-Dalsgaard et al. 1995) and it can also be used for solar-type stars (Monteiro et al. 2000). The expression

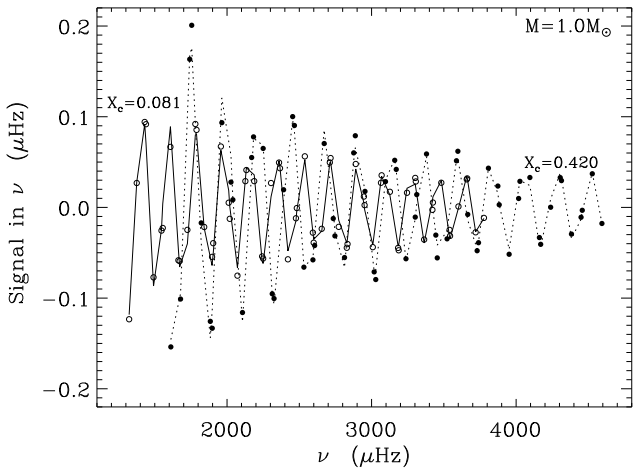

Figure 3. Signal in the frequencies due to the border of the convective envelope in two models of different ages for a star of a solar mass.

of the signal from one such transition layer for very low degree modes can be written as (see Monteiro et al. 2000)

$$A(\omega)\cos\left[2(\omega\bar{\tau}_{\rm d}+\phi_0)\right] \ , \qquad (4)$$

where ω is the frequency of the mode (ω=2$\pi\nu$), $A(\omega)$ the amplitude of the signal, $\bar{\tau}_{\rm d}$ an acoustic depth and ϕ_0 a phase. The quantities $A(\omega)$ and $\bar{\tau}_{\rm d}$ are determined by the sharpness of the transition and its acoustic location, respectively.

When determining the large separation, care should be taken to take account of additional contributions which are not included in the asymptotic analysis. Therefore we have removed the major contribution which dominates at the lower range of frequencies (low mode order) due to the presence of the second helium ionization (e.g. Monteiro & Thompson 1998, Pérez Hernández & Christensen-Dalsgaard 1998). We have done so by fitting to $\Delta\nu$ the sum of a smooth component $\Delta\nu_a(\nu)$ and a component of the form

$$\Delta\nu_b \propto \frac{\sin^2(\beta\omega)}{\omega}\ \cos\left[2(\bar{\tau}_d\omega+\phi_0)\right] \ , \qquad (5)$$

which is a special case of an oscillatory signal as described by Eq. (4). Here the quantities β and $\bar{\tau}_d$ characterise the second helium ionization zone (width and acoustic depth respectively - see Monteiro & Thompson 1998).

Figure 1 illustrates our method: the smooth component ($\Delta\nu_a$) is shown as a dashed line, and results from a fit of the form $\Delta\nu\equiv\Delta\nu_a+\Delta\nu_b$. In order to calibrate the dependence of the large separation on the global properties of the star we consider its value at ν=2500μHz. We keep only the smooth component to calculate

$$\Delta\bar{\nu} \equiv \Delta\nu_a(\nu{=}2500\mu{\rm Hz}) \ . \qquad (6)$$

Figure 2 shows the small frequency separations for l=0 and the fit we consider in order to define the value at 2500μHz as:

$$\delta\bar{\nu} \equiv \delta\nu(\nu{=}2500\mu{\rm Hz}) \ . \qquad (7)$$

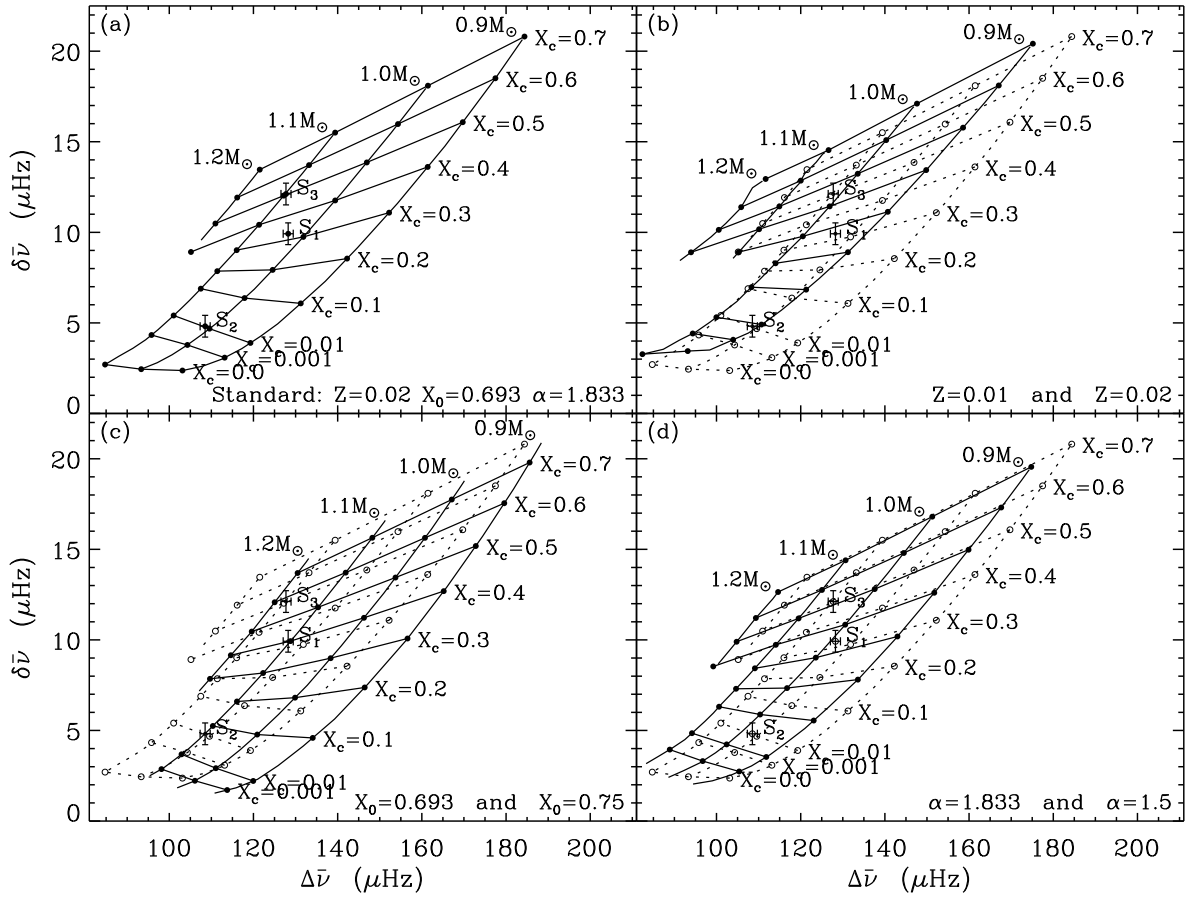

Figure 4. (a) The CD diagram for evolutionary sequences of 0.9, 1.0, 1.1 and 1.2 solar mass stars - all the models have Z=0.02, X_0=0.693 and α=1.833 (see Section 3.1). The test stars (see Table 1) are also indicated in all panels with 3-sigma error bars. (b) CD diagram for models with Z=0.01 (continuous line). The "standard" diagram from panel (a), with Z=0.02 (dotted lines) is shown as a reference. (c) CD diagram for models with X_0=0.75 (continuous line). The "standard" diagram with X_0=0.693 (dotted lines) is also shown. (d) CD diagram for models with α=1.5 (continuous line). Our "standard" diagram with α=1.833 (dotted lines) is also shown.

Figure 3 illustrates the oscillatory signal from the base of the convection zone in two stellar models. The signal is extracted from the frequencies in the manner described by Monteiro et al. (1994) and Monteiro et al. (2000). For comparing the properties of convective borders of stars of different age and mass we use the value of the signal amplitude at frequency $\tilde{\omega}/2\pi$=2500μHz, by defining $A_{\rm d}\equiv A(\tilde{\omega})$. The measured quantities $A_{\rm d}$ and $\bar{\tau}_{\rm d}$ provide direct constraints on the stratification and location of the base of the convective envelope of the star.

3. Dependence on stellar mass and age

Evolutionary sequences of different-mass stars have been calculated as described by Christensen-Dalsgaard (1993a). In particular, the EFF equation of state (Eggleton et al. 1973) was used, as well as OPAL92 opacities (Rogers & Iglesias 1992).

3.1. The CD diagram

From a set of evolutionary sequences of stellar models we compute the stars' eigenfrequencies and hence position each star on a $(\Delta\bar{\nu}, \delta\bar{\nu})$ diagram - the so-called CD Diagram. As a reference case, we use a "standard" set of parameters (Z=0.02, initial hydrogen abundance X=0.693, mixing-length parameter α=0.183); the resulting diagram is shown in Fig. 4(a). A star's position in the diagram depends on its mass and its age.

Any unknown star whose large and small separations have been calculated in the same way can now be located within this diagram and hence its mass and age can be estimated. This can be done independently of any other observational information about the star. But any property which is known for the models in the calibration set may be estimated similarly, e.g. luminosity or effective temperature. Of course all such calibration may be inaccurate if the other physics of the star is unlike that used in the

models used to construct the diagram. Therefore we consider the effect on the CD diagram of modifying aspects of the physics of the stellar models, specifically the metal abundance Z, the hydrogen abundance X, and the mixing length parameter α.

Figure 4(b) shows the CD diagram obtained using models with a heavy element abundance Z=0.01, the other parameters having the "standard values". Figure 4(c) shows the CD diagram obtained using models with an initial hydrogen abundance X_0=0.75, the other parameters have their standard values. Finally, Fig. 4(d) illustrates the effect of using a mixing-length parameter α=1.5 with other parameter values as standard.

Calibrating with each such CD diagram will in general give a different estimate of the mass and age of the star. However, if other quantities are also known independently of seismology for the unknown star, such calibration provides a consistency check and may reveal inconsistencies between the unknown star and the physics assumed for the calibration models.

3.2. Convective borders

The amplitude and acoustic-depth parameters deduced for a convective border also depend on the mass and age of the star. In order to illustrate the dependence on mass and age we consider again the same sequence of models of different masses evolved from the ZAMS to the end of the main sequence (see above). Here we assume that the central helium abundance X_c is a measure of the age of the star in the main sequence. No type of overshoot has been included in this set of evolutionary sequences. In Fig. 5 the behaviours of both parameters are shown for all models.

A large part of the variation of the large separation, the amplitude and the acoustic depth arise from the variation of the mass M and radius R of the stars whereby quantities with dimensions of frequency vary as $\sqrt{M/R^3}$. (The variation of the small separation is affected more by nonhomologous variations in structure.) To illustrate that, in Fig. 6 we rescale the amplitude and acoustic depth

$$A_{\rm d} \times \left[\frac{M/M_\odot}{(R/R_\odot)^3}\right]^{-1/2} \qquad \text{and} \qquad \bar{\tau}_{\rm d} \times \left[\frac{M/M_\odot}{(R/R_\odot)^3}\right]^{1/2} \quad (8)$$

to reveal other variations due to the changing size of the envelope, which affects not only the location but also the sharpness of the boundary.

4. Test stars - observational data

By way of illustration we consider three test stars which were provided from one co-author to another as a blind test. Table 1 lists all the information and errors bars that were assumed as known for the test stars.

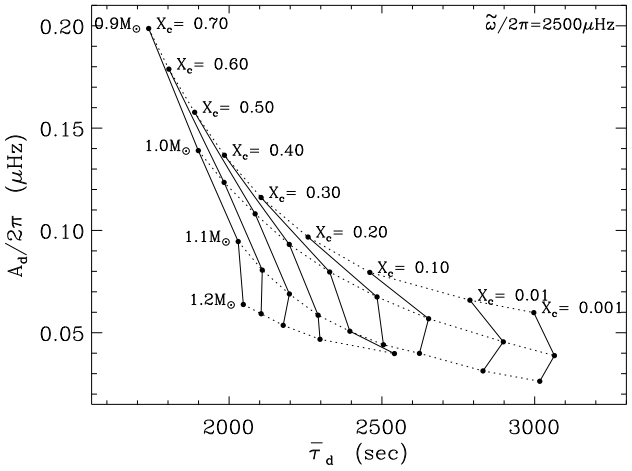

Figure 5. Diagram of the amplitude of the signal versus the acoustic depth locating the base of the convection zone for our 'reference' set of models. The dotted lines indicate models of the same mass while continuous lines are models with the same central hydrogen abundance X_c, as indicated.

4.1. The CD-Diagram fits

We can use the procedure described in Section 3 to analyse these data in terms of our CD diagrams; the positions of the stars have been shown in Fig. 4. The inferred values of the stellar parameters are given in Table 2. The errors bars have been estimated by determining the uncertainties due only to the observational uncertainties for the frequencies. As well as M and X_c, the effective temperature and luminosity of the star can be calibrated from the evolutionary tracks corresponding to the CD diagram. These values are also shown in Table 2.

4.2. Fits for the convective borders

By isolating the signal in the frequencies, with a fit of the expression (4) we determine a value for the amplitude $A_{\rm d}$ and the acoustic location $\bar{\tau}_{\rm d}$. The results are given in Table 3. The error bars have been estimated in accordance with Monteiro et al. (2000) from the error of 0.1μHz in the individual frequencies.

Table 3. Parameters of the signal as found from fitting the expression of the signal to the frequencies of the stars.

Star	$\bar{\tau}_{\rm d}$ (sec)	$A_{\rm d}/2\pi$ (μHz)
S_1	2201±45	0.103±0.014
S_2	2404±42	0.045±0.008
S_3	2272±73	0.164±0.012

Table 1. Data provided for the seismic analysis of the stars. The values of the mode degree l and order n for all frequencies considered are listed, to show what frequency data we have considered. In order to simulate a real observation we also consider as known the luminosity L of the star, its effective temperature $T_{\rm eff}$ and its metallicity $Z_{\rm s}/X_{\rm s}$.

Star	l	n	$\sigma(\nu)$ (μHz)	$L/L_\odot$	$T_{\rm eff}(K)$	$Z_{\rm s}/X_{\rm s}$
S_1	0	14-32	0.1	1.186±0.036	5810.6±50.0	0.0274±0.0014
	1	13-29				
	2	16-28				
S_2	0	14-32	0.1	1.355±0.041	5725.0±50.0	0.0229±0.0011
	1	13-29				
	2	15-30				
	3	16-28				
S_3	0	14-32	0.1	1.259±0.038	5947.9±50.0	0.0282±0.0014
	1	13-29				
	2	15-30				
	3	16-28				

Table 2. Mass and central hydrogen abundance for the test stars as found from the CD diagrams shown in Fig. 4 (a), (b), (c) and (d) respectively. Also given are the values of the luminosity and effective temperature inferred from the same sets of calibration models.

Star	$\Delta\bar{\nu}$ (μHz)	$\delta\bar{\nu}$ (μHz)	Physics	$M/M_\odot$	$X_{\rm c}$	$L/L_\odot$(cal)	$T_{\rm eff}$(cal)
S_1	128.3	9.92	*Standard*	1.035±0.009	0.330±0.018	1.166	5859
			Z=0.01	0.949±0.009	0.283±0.017	1.279	6085
			Y=0.75	1.104±0.010	0.403±0.019	1.108	5729
			α=1.5	0.992±0.009	0.347±0.015	0.948	5606
S_2	108.5	4.82	*Standard*	1.014±0.012	0.016±0.007	1.444	5836
			Z=0.01	0.910±0.012	0.011±0.007	1.517	6014
			Y=0.75	1.099±0.012	0.067±0.014	1.436	5759
			α=1.5	0.975±0.011	0.045±0.009	1.202	5600
S_3	127.7	12.12	*Standard*	1.098±0.010	0.504±0.023	1.328	5996
			Z=0.01	1.015±0.010	0.457±0.023	1.460	6231
			Y=0.75	1.177±0.010	0.585±0.020	1.286	5865
			α=1.5	1.060±0.010	0.526±0.020	1.104	5746

5. Combined inferences

With the values found above we can now attempt to estimate what type of stars we have as blind tests.

5.1. Masses and ages

The first point to note is that the masses and central hydrogen abundances inferred for our test stars, given in Table 2, are discrepant. This shows the sensitivity of the calibration based on the frequency separations to the physics assumed when the CD diagram is constructed. From the large and small separations alone there is no way to discriminate between these different inferences.

However, for our test stars, and we expect for future asteroseismic target stars also, we have additional observational constraints. In the present case we have independent estimates of the luminosities and temperatures of the stars. These quantities can also be estimated for the calibration sets and hence internal inconsistencies may be revealed. Specifically, we show in Fig. 7 the specified locations of the test stars (cf. Table 1) with the associated error boxes; in addition, the figure shows those values of $T_{\rm eff}$ and L that would be obtained from the values of M and $X_{\rm c}$ inferred from the four CD diagrams in Fig. 4 (see Table 2). This allows us to test the consistency of our inferences.

As given in Table 1 we also have the values of $Z_{\rm s}/X_{\rm s}$ for each star. This quantity complements Fig. 7 by providing an extra consistency test.

Using our standard CD diagram (Fig. 4) gives consistent values for S_1 (compare values of L and $T_{\rm eff}$ in Tables 1 and 2). We conclude that star S_1 has a mass $M/M_\odot$=1.035±0.009, and a central hydrogen abundance

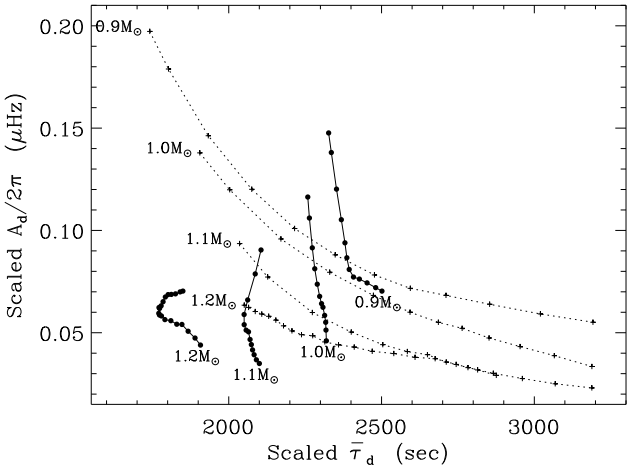

Figure 6. Diagram of $A_{\rm d}\times\sqrt{R^3/M}$ versus $\bar{\tau}_{\rm d}\times\sqrt{M/R^3}$, where R and M are surface radius and total mass of the stars, in solar units. The dotted lines show the original values, without the homology scaling factor. The plot illustrates how much of the variation of these two parameters is not homologous. Note that the amplitude decreases with increasing age.

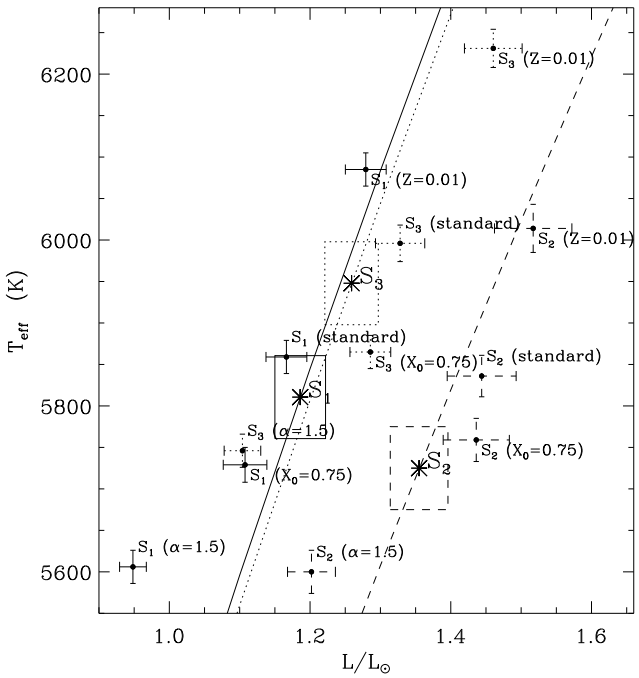

Figure 7. Luminosity (in solar units) and effective temperature for the test stars. The large symbols with error boxes show the 'observed' values provided in Table 1. The remaining points have been determined from the inferred $(M, X_{\rm c})$ for each of the four sets of reference models, using the appropriate evolutionary tracks. The standard calibration case has Z=0.02, X_0=0.693 and α=0.183. The lines indicate models of constant radius, as determined from the observations of the luminosity and effective temperature for each test star.

of $X_{\rm c}$=0.330±0.018. The star appears to be consistent with our calibration models, which have a heavy element abundance of 0.02 and an initial abundance of hydrogen of 0.6928. We note that the specified value of $Z_{\rm s}/X_{\rm s}$ is consistent with this conclusion.

For case S_2, the luminosity obtained by calibration to our standard CD diagram (Table 2) is larger than the star's observed luminosity (Table 1). Likewise the effective temperature is discrepant. We conclude that the physics and/or abundances of S_2 are not the same as those used in the calibration models. If instead we use Z=0.01, the calibrated values of L and $T_{\rm eff}$ are even more discrepant. In order to reconcile the values we can either increase the value of Z or increase the value of X_0. Taking into consideration the measured metalicity $Z_{\rm s}/X_{\rm s}$ the best option would be to increase X_0. We can also decrease slightly the value of α, corresponding to saying that this star has a higher value of X_0 and a lower value of α. We clearly need to increase the radius (and hence, by homology, also increase the mass) of the star that comes out of the standard CD diagram (Fig. 4). Taking these factors in consideration we would say the global properties for S_2 are that $M/M_\odot$=1.05±0.01 and $X_{\rm c}$<0.1. For this star we should build first a more adequate CD diagram before calculating its global properties.

For case S_3 the value of the luminosity obtained by our standard calibration (Table 2) is again higher than actually observed, though the calibrated and observed temperatures are marginally consistent within the observational error bars. This star seems to indicate that it has a high $Z_{\rm s}/X_{\rm s}$. It probably also has a higher value of X_0 which is associated with a lower value of α. That is, we would say this star has Z=0.021 and $X_0\simeq$0.72. If that is the case then we may propose that this star has $M/M_\odot$=1.1±0.02 and $X_{\rm c}\simeq$0.55±0.02. Again, we should iterate on the physics in order to get a better CD diagram for this star.

5.2. Convective borders

Assuming that we have been successful with the determination of the stellar mass and central helium abundance, we now try to determined the main characteristics of these stars at the base of their convective envelopes. Fig. 8 shows the measured quantities $A_{\rm d}$ and $\bar{\tau}_{\rm d}$ for the test stars, and the values expected for our reference set of models. For comparison we also show what values we would expect in the reference models with no overshoot, for stars with masses and ages as determined for S_1, S_2 and S_3 from the CD diagram analysis. Note that, rather than using our reference-case models, it would be more consistent to

calibrate against model sequences computed according to our best-fit parameters determined in Section 5.1.

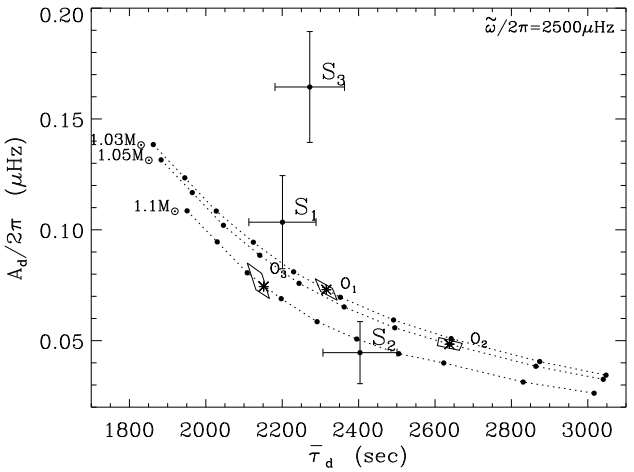

Figure 8. Diagram of the amplitude of the signal versus the acoustic depth locating the base of the convection zone for our test stars (S_1, S_2 and S_3). The values we would expect to measure in models with no overshoot, considering the mass and age we have previously determined for these stars, are also indicated (O_1, O_2 and O_3).

Both models S_1 and S_3 show a higher amplitude than expected and thus appear to differ from the corresponding references models in terms of the stratification at the base of the convective envelope. An adiabatically stratified overshoot layer of $0.2H_p$ for S_3 and $0.1H_p$ for the less massive star S_1 could account for this. These limits were calculated using the dependence of the amplitude on overshoot, for different ages, as given by Monteiro et al. (2000). For S_1 the measured value of $\bar{\tau}_{\rm d}$ is smaller than expected, which is not what we should see with the presence of an overshoot layer. That may indicate that the sharpness we measure in the amplitude could be associated with diffusion at the base of the envelope, and not overshoot as said above. (In the blind test, the investigator did not provide error bars on the above-quoted overshoot values. In fact we note a posteriori that the remarked-upon deviation of S_1 from the corresponding reference model is only at the 1-σ level.)

Regarding S_2 there is no difference in amplitude indicating that the smoothness of the transition in S_2 is similar to that in the reference models. However, there is an indication of a smaller acoustic depth (at the 2-σ level), which we could attribute to the atmospheric contribution to $\bar{\tau}_{\rm d}$ (a different reflecting layer at the top of the star will introduce a shift in $\bar{\tau}_{\rm d}$ of up to about 100 sec). Overshoot that is not adiabatically stratified can also introduce a signal which differs from the expected values mainly in the acoustic depth, and not in amplitude. But such a fuzzy extension by overshooting would tend to increase $\bar{\tau}_{\rm d}$ relative to our reference models, and so does not appear to be relevant here.

6. The truth

After the completion by one of the authors of the preceding analysis of the test data, the true properties of the underlying models, presented in Table 4, were revealed. The following additional comments about the models may be made:

S_1 - This was constructed using the same physics and parameters as our 'standard' reference set. As concluded, the inference of M and $X_{\rm c}$ was quite secure.

S_2 - This model used the OPAL equation of state (Rogers, Swenson & Iglesias 1996) and OPAL95 opacities (Iglesias & Rogers 1996), and included diffusion and settling of helium and heavy elements.

S_3 - This used the same physics and parameters as our 'standard' reference set, except for including overshoot from the convective envelope, over 0.2 pressure scale heights.

7. Discussion

Our process of inference proceeds in two steps: firstly, estimating the stars' masses and ages with the CD diagram, and then investigating the sharpness and location of the convective borders.

7.1. The CD-Diagram

We have demonstrated that the physics adopted for the models used to construct the CD diagram has an effect on the mass and central hydrogen abundance inferred from the large and small separations. We have quantified this effect for three possible changes: the heavy-element abundance, the initial hydrogen abundance; and the mixing-length parameter. We have also quantified the uncertainties in the seismic determinations due to observational errors in the frequencies.

We have shown how additional observational data (specifically a star's luminosity and effective temperature) complement the seismic data and thus enable the mass and central hydrogen abundance to be better determined. Such additional constraints may also permit inconsistencies in the physics to be revealed. Thus introducing information from additional observables (luminosity, effective temperature, chemical abundances, surface gravity, ...) can raise the degeneracy that otherwise exists when attempting to calibrate stars using just two seismic measurements, the large and small separations (e.g. Brown et al. 1994).

Of course it should also be borne in mind that the frequency separations actually depend on frequency (e.g.

Table 4. True masses and central hydrogen abundances for the test stars for which inferences were attempted. Also indicated are the size of the overshoot layer ($\ell_{\rm ov}$) in units of the local pressure scale-height (H_p), which has been modelled as being adiabatic, and whether or not the star has settling/diffusion (Dif.) and uses different opacity tables and equation of state (Phys.) from our reference models.

Star	$\Delta\bar{\nu}$ (μHz)	$\delta\bar{\nu}$ (μHz)	$M/M_\odot$	$X_{\rm c}$	$\ell_{\rm ov}/H_p$	Dif.	Phys.
S_1	128.3	9.92	1.033	0.333	0.0	no	no
S_2	108.5	4.82	1.000	0.017	0.0	yes	yes
S_3	127.7	12.12	1.100	0.521	0.2	no	no

Figs 1 and 2) and are not simply two numbers: this variation also contains valuable information about the objects of study which we have not as yet exploited in this study.

7.2. The convective borders

We have had fair success in the first step. That is very important in order to be able to perform the comparison of the amplitude and the acoustic depth of the signal with a set of models of solar-type stars of different ages, as we have done here.

We anticipate that difficulties of interpretation in the second step may arise from the opposing contributions of different aspects of the physics relevant for the base of the envelope. The frequencies only provide us a measure of the sharpness of that transition. This aspect is dependent on every aspect of the physics at play at that location, including convection and overshoot, the equation of state, opacities, diffusion and settling, as well as aspects not included in our present models but undoubtedly at play in real stars (magnetic fields, rotation, etc.). Therefore to translate some of the values we find here for the amplitude we must make sure that we have reproduced as closely as possible in our models the physics of the star. That also includes the CD diagram analysis where such an iteration must be done. For a star with a large adiabatically stratified overshoot layer we had no problems identifying its presence (S_3). This information could and should be fed back into the CD Diagram analysis in order to improve the estimates provided for the mass and central helium abundance.

The inferences for the star S_2 with modified physics were also reasonably successful. The initial guess was that the apparently slightly anomalous value of $\bar{\tau}_{\rm d}$ was due to the surface contribution. In fact, settling, a different equation of state and different opacity tables in this model have changed the expected value of $\bar{\tau}_{\rm d}$, but we do have difficulties in determining that without going back to the CD diagram where an iteration on the physics could lead us to adapt the physics in order to satisfy all observational constraints.

Finally, the case of S_1 was on the face of it a little disappointing. The step of estimating the mass and age was very successful, and indeed the star had input physics matching that of the grid of reference models. But the inferences about the base of its convective envelope were wide of the mark. The lesson, which is brought home most forcefully in a blind test, is that one can overinterpret noisy data. As we saw with hindsight, the inferred values of the amplitude and acoustic depth for this star are only just over one standard deviation from the values expected from the reference models.

Acknowledgements

This work was supported in part by the Portuguese Fundação para a Ciência e a Tecnologia, by the Danish National Research Foundation through its establishment of the Theoretical Astrophysics Center and by the UK Particle Physics and Astronomy Research Council.

References

Basu S., Antia H.M., Narasimha D., 1994, MNRAS 267, 209
Brown T.M., Christensen-Dalsgaard J., Mihalas B., Gilliland R.L., 1994, ApJ 427, 1013
Christensen-Dalsgaard J., 1993a, in Inside the Stars. IAU 137, (Eds) Weiss W.W. & Baglin A., A.S.P. Conf. Ser., Vol. 40, 483
Christensen-Dalsgaard J., 1993b, in Proc. GONG 1992: Seismic investigation of the Sun and stars, (Ed.) Brown T.M., A.S.P. Conf. Ser., Vol. 42, 347
Christensen-Dalsgaard J., Monteiro M.J.P.F.G., Thompson M.J., 1995, MNRAS 276, 283
Eggleton P.P., Faulkner J., Flannery B.P., 1973, A&A 23, 325
Gough D.O., 1987, Nature 326, 257
Iglesias C.A., Rogers F.J., 1996, ApJ 464, 943
Monteiro M.J.P.F.G., Thompson M.J., 1998, in Structure and Dynamics of the Interior of the Sun and Sun-like Stars, (Eds) S.G. Korzennik & A. Wilson, ESA SP-418, ESA Publications Division, p. 819
Monteiro M.J.P.F.G., Christensen-Dalsgaard J., Thompson M.J., 1994, A&A 283, 247
Monteiro M.J.P.F.G., Christensen-Dalsgaard J., Thompson M.J., 2000, MNRAS 316, 165
Pérez Hernández F., Christensen-Dalsgaard J., 1998, MNRAS 295, 344
Rogers F.J., Iglesias C.A., 1992, ApJS 79, 507
Rogers F.J., Swenson F.J., Iglesias C.A., 1996, ApJ 456, 902
Roxburgh I.W., Vorontsov S.V., 1994, MNRAS 268, 880